Was UV spectral solar irradiance lower during the recent low sunspot minimum?

Article

Published Version

Was UV spectral solar irradiance lower during the recent low sunspot minimum?

Mike Lockwood[1,2]

Received 11 July 2010; revised 3 May 2011; accepted 10 May 2011; published 16 August 2011.

[1] A detailed analysis is presented of solar UV spectral irradiance for the period between May 2003 and August 2005, when data are available from both the Solar Ultraviolet Spectral Irradiance Monitor (SUSIM) instrument (on board the Upper Atmosphere Research Satellite (UARS) spacecraft) and the Solar Stellar Irradiance Comparison Experiment (SOLSTICE) instrument (on board the Solar Radiation and Climate Experiment (SORCE) satellite). The ultimate aim is to develop a data composite that can be used to accurately determine any differences between the "exceptional" solar minimum at the end of solar cycle 23 and the previous minimum at the end of solar cycle 22 without having to rely on proxy data to set the long-term change. SUSIM data are studied because they are the only data available in the "SOLSTICE gap" between the end of available UARS SOLSTICE data and the start of the SORCE data. At any one wavelength the two data sets are considered too dissimilar to be combined into a meaningful composite if any one of three correlations does not exceed a threshold of 0.8. This criterion removes all wavelengths except those in a small range between 156 nm and 208 nm, the longer wavelengths of which influence ozone production and heating in the lower stratosphere. Eight different methods are employed to intercalibrate the two data sequences. All methods give smaller changes between the minima than are seen when the data are not adjusted; however, correcting the SUSIM data to allow for an exponentially decaying offset drift gives a composite that is largely consistent with the unadjusted data from the SOLSTICE instruments on both UARS and SORCE and in which the recent minimum is consistently lower in the wave band studied.

Citation: Lockwood, M. (2011), Was UV spectral solar irradiance lower during the recent low sunspot minimum?, *J. Geophys. Res.*, *116*, D16103, doi:10.1029/2010JD014746.

1. Introduction

[2] The recent solar minimum between sunspot cycles 23 and 24 has set record lows for many solar parameters that have been measured since the start of the space age [see reviews by *Lockwood*, 2010; *Russell et al.*, 2010]. Indeed, parameters available for before the onset of space observations (for example, the annual mean sunspot number, the fraction of sunspot-free days, open solar flux derived from geomagnetic activity [*Lockwood et al.*, 1999, 2009a]) show that this solar minimum has been lower than any since about 1920. By studying cosmogenic isotope records, *Abreu et al.* [2008] showed that the space age has been within a grand maximum of solar activity which has been unusually long in duration. From the distribution of durations of previous grand maxima over the past 9300 years, these authors predicted that the current one will soon come to an end. This conclusion is supported by *Lockwood et al.* [2009b], who showed that the recent solar minimum is part of a decline in solar activity which began at a grand peak in 1985 [*Lockwood and Fröhlich*, 2007].

[3] From the viewpoint of climate change studies, a return to 1920 conditions is highly significant. Both the GISS [*Hansen et al.*, 1999] and HadCRUT3v [*Brohan et al.*, 2006] reconstructions show that the change in global mean air surface temperature (GMAST) between 1920 and 2009 is near 0.76°C. This is a sizable fraction of the total estimated change in GMAST since preindustrial times. Thus it becomes important to quantify changes in the total solar irradiance (TSI) and UV spectral solar irradiance (SSI) in the last solar minimum compared to previous ones, as this can help to evaluate the solar contribution to both global and regional climate change since 1920. *Fröhlich* [2009] reports that the TSI was slightly lower in the recent minimum compared to the previous two minima. However, it must be stressed that such studies require a composite of the data from several different instruments and that these instruments require accurate intercalibration. In addition, the instruments degrade, and whereas some have been self-calibrating, earlier instruments require retrospective recalibration. The

[1]Space Environment Physics Group, Department of Meteorology, University of Reading, Reading, Berkshire, UK.
[2]Space Science and Technology Department, Rutherford Appleton Laboratory, Didcot, Oxfordshire, UK.

0148-0227/11/2010JD014746

three available TSI data composites are termed PMOD [*Fröhlich*, 2006], ACRIM [*Willson and Mordvinov*, 2003], and IRMB [*Dewitte et al.*, 2004]. *Lockwood* [2010] has studied the decadal-scale trends inherent in these three composites. For IRMB, the trend is upward and so anti-correlated with the sunspot number, R: the variation on decadal scales with R is linear and extrapolated to $R = 0$ gives a Maunder minimum value of the TSI that is 1.2 W m^{-2} higher than modern average values. This runs counter to most expectations of solar behavior during the Maunder minimum and European "Little Ice Age." The trend in the ACRIM composite bears almost no relation to R, being initially upward and then downward, whereas average sunspot numbers have declined since 1985 [*Lockwood and Fröhlich*, 2007]. On the other hand, the PMOD composite matches the long-term trend in R well, although the variations are not linearly related. Extrapolation using the PMOD composite suggests that TSI was lower than present-day values by 1.3 Wm^{-2} during the Maunder minimum, consistent with recent TSI reconstructions [*Krivova et al.*, 2007; *Wang et al.*, 2005]. Of the three composites, PMOD contains the largest number of detailed corrections for instrumental performance and stability and overall agrees best with the Spectral and Total Irradiance Reconstructions (SATIRE) analysis of solar magnetograph data which accounts for magnetic solar surface effects [*Wenzler et al.*, 2009]. Recent analysis shows that the SATIRE modeling reproduces the fall in the PMOD TSI into the recent solar minimum [*Krivova et al.*, 2011] but indicates that the previous minimum in 1996 was overestimated in the PMOD composite by roughly 0.2 Wm^{-2}, roughly the difference between that minima and the recent one reported by *Fröhlich* [2009]. This could also mean that the 1996 minimum was slightly lower than its predecessor. Thus it may be that solar minimum TSI has declined very slightly over the last three minima, but the uncertainties in the calibration of measurements remain.

[4] For solar UV spectral irradiance the situation is even more confused. The decline in UV emission during the descent into this exceptional solar minimum was monitored by the SIM and SOLSTICE instruments on board the SORCE satellite (see section 2) and revealed a larger change in the UV emissions at many wavelengths [*Harder et al.*, 2009] than had been seen by prior instruments at the corresponding phase of previous solar cycles [*Lean*, 2000; *DeLand and Cebula*, 2008], particularly at the wavelengths responsible for stratospheric ozone production and heating. In addition, wavelengths in visible and near-IR bands showed the opposite trend to the UV. By modeling the effect of these spectral changes, *Haigh et al.* [2010] found evidence that supports the SORCE data in ozone abundances measured by the Aura-MLS satellite. However, as for TSI, attention must be paid to the intercalibration of the instruments. *Snow et al.* [2010] and *Lean* [2011] use a proxy for the UV emission (the Mgii index) as a framework on which to bring the different UV data sets together. These analyses did not show any sizable change of the recent solar minima, compared to data composites covering previous minima. This is considerably different from the results obtained by *Harder et al.* [2009] and *Haigh et al.* [2010]. *Lockwood et al.* [2010b] used two simple intercalibration methods between the SORCE data and the composite of *DeLand and Cebula* [2008] and inferred that the change between the minima was somewhat smaller than in the *Harder et al.* [2009] and *Haigh et al.* [2010] studies but larger than that derived from the proxy-based reconstructions by *Lean* [2000] and by *Snow et al.* [2010]. However, these authors noted that the results depended strongly on the intercalibration procedure used.

[5] Care must be taken when using proxy reconstructions, based on one or several solar indices, to evaluate the long-term changes. *Dudok de Wit et al.* [2009] have studied the correlations between SSI and various proxies and found that the performance of the proxy varies with the time scale considered. Hence a good correlation over short time scales does not necessarily mean that the correlation will also apply to the long-term changes. Hence proxies that do not show long-term change and correlate well on short time scales have the potential to suppress genuine long-term changes in total or spectral irradiance.

[6] The possibility of long-term change in UV solar irradiance has considerable implications for understanding regional climate change in some parts of the world. Solar UV changes have considerable effect on the distribution of temperatures and winds in the stratosphere [see review by *Gray et al.*, 2010]. There is growing evidence that dynamical coupling across the tropopause means that these stratospheric changes can have a disproportionate influence on the underlying troposphere ("top down" solar effects) [e.g., *Matthes et al.*, 2006]. Tropospheric jet streams have been predicted to be particularly sensitive to the solar forcing of the stratosphere [*Haigh*, 2003]. Disturbances to the stratospheric polar vortex [*Gray et al.*, 2004], which are observed to propagate downward and evolve into perturbations to the tropospheric jets [*Baldwin and Dunkerton*, 1999], have been proposed as a potential mechanism [see *Gray et al.*, 2010]. However, the coupled nature of these stratospheric/tropospheric disturbances means that the fact that the disturbances appear first in the stratosphere does not necessarily mean that the stratosphere changes are driving those in the troposphere below [*Plumb and Semeniuk*, 2003]. A second proposed mechanism is that solar-induced stratospheric changes may influence the refraction of upward-propagating tropospheric eddies [*Kushner and Polvani*, 2004; *Simpson et al.*, 2009]. Modeling [*Shindell et al.*, 2001] and observations [*Perlwitz and Harnik*, 2003] have indicated that perturbations can descend from the stratosphere to the surface by altering the propagation of planetary waves coming up from the surface. Definitive identification of these top-down solar influences on the troposphere is difficult; however, models show that the stratosphere has the potential to play a crucial role in regional climates. For example, *Scaife et al.* [2005] have demonstrated that stratospheric trends over recent decades, along with downward links to surface, are indeed strong enough to explain much of the prominent trend in the North Atlantic Oscillation (NAO) between the 1960s and the 1990s, with implications for regional climate in Europe, particularly in winter. Observational studies suggest that a secular change in UV irradiance may be having an effect on regional climates. *Woollings et al.* [2010] have shown that the jet stream blocking phenomenon in the mid Atlantic and over Europe, and consequent effects on surface temperatures in the Eurasian sector, is better described by solar indices that do show a secular change as well as a solar cycle variation. The same conclusion was reached by *Lockwood et al.* [2010b]

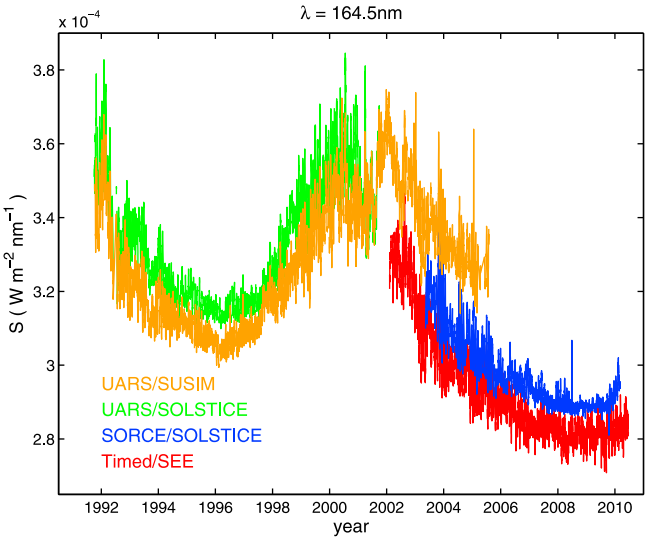

Figure 1. Published solar spectral irradiance $S(\lambda)$ data for an example 1 nm wide band around $\lambda = 164.5$ nm: UARS/SUSIM (orange), UARS/SOLSTICE (green), SORCE/SOLSTICE (blue) and Timed/SEE (red). The figure illustrates the "SOLSTICE gap" between the end of the available UARS/SOLSTICE data and the start on SORCE/SOLSTICE observations.

from a multiple regression study of zonal means of tropospheric and stratospheric zonal winds and temperatures. These studies provide a potential explanation of the link between long-term solar change and European winter temperatures, as for example, discussed by *Lockwood et al.* [2010a].

2. Solar UV Spectral Irradiance Data

[7] Figure 1 shows daily means of the available data series for one 1 nm wide wavelength (λ) band. This example is the band centered on $\lambda = 164.5$ nm and values for a mean solar distance of 1 astronomical unit (AU) are given in units of W m^{-2} nm^{-1}. The data sequence shown in orange is from the SUSIM (Solar Ultraviolet Spectral Irradiance Monitor) instrument on UARS (the Upper Atmosphere Research Satellite) [*Brueckner et al.*, 1993]. This absolutely calibrated, dual-dispersion, dual-spectrometer instrument was mounted on the UARS Solar-Stellar Pointing Platform (SSPP) which normally tracked the Sun for at least 35 min in each of the sixteen 90 min UARS orbits per day. SUSIM measured over the wavelength range 115 to 411 nm. In-flight calibration used stable deuterium lamps that were periodically scanned and elements in the instrument optical path could be swapped and hence calibrated. The plot uses the level 3 data and known sources of error (in order of importance) are [*Woods et al.*, 1996, 1998]: response degradation estimation, stray light, pre-flight calibration uncertainties in absolute values, wavelength assignment, pointing errors, detector gains and temperature corrections, signal measurement random error, and dark signal measurement. The SUSIM data cover the interval October 1991 to August 2005. This gives SUSIM data overlap with data from the Solar Radiation and Climate Experiment (SORCE) and the Thermosphere Ionosphere Mesosphere Energetics and Dynamics (TIMED) satellites.

[8] The Solar Stellar Irradiance Comparison Experiment (SOLSTICE) instrument on the UARS spacecraft measured solar spectral irradiance reliably from October 1991 to September 2001, covering the wavelength range $\lambda = 119$–420 nm [*Rottman*, 2000]. The typical uncertainty of the relative irradiance is less than 1 percent for solar measurements. The green line in Figure 1 shows UARS/SOLSTICE Level 3 products which have been filtered to remove data which may be questionable due to larger than normal pointing uncertainty, contamination by the South Atlantic Anomaly or atmospheric absorption, and which are significantly outside the range of values expected over a solar cycle or observed over the last several orbits. As shown in Figure 1, the UARS/SOLSTICE data not overlap with data from either SORCE or TIMED. In the present study these data are used before 2001 and are intercalibrated with SUSIM data over the interval 1999–2001.

[9] The two SOLSTICE instruments on board the SORCE satellite measure spectral irradiance from 115 nm to 320 nm with a resolution of 1 nm [*McClintock et al.*, 2000; 2005a; 2005b] and the SIM (Spectral Irradiance Monitor) instrument [*Harder et al.*, 2000; 2005a; 2005b] measures spectral irradiance from 310 nm to 2400 nm with a resolution varying from 1 to 34 nm. There is an additional SIM channel covering the 200–300 nm band which provides additional calibration of SOLSTICE. SORCE/SOLSTICE makes daily measurements and compares them to the irradiance from an ensemble of 18 stable early type stars. The SOLSTICE-A MUV (180–310 nm) channel observations have been corrected for degradation by cross-calibration to SOLSTICE-B. Only SOLSTICE-B makes stellar calibration observations, because of a known misalignment of SOLSTICE-A's slit aperture. Weekly comparisons of the data from the A and B instruments are used to correct any drift between the two. Corrections for differences in field of view between solar and stellar modes at four wavelengths have been included. This paper is concerned with the relative, rather than the absolute accuracy which for the relevant MUV band (180–310 nm) is estimated to be about 0.2–2.6% per year [*McClintock et al.*, 2000, 2005a, 2005b]. Known uncertainties are: a scattered light correction applied to the data (a ~1% effect at some wavelengths); the characterization of the instrument's susceptibility to detector temperature changes; and that MUV measurements made after late January 2006 exhibit a pointing-related discontinuity that is associated with an instrument mechanism anomaly (a correction has been applied but a small discontinuity remains at some wavelengths). Data were obtained prior to May 2003 but instrument artifacts related to instrument pointing mean these data have not yet been fully corrected and are not used here. The blue line in Figure 1 shows version 9 of the SORCE/SOLSTICE data. These data continue to the time of writing.

[10] The Solar EUV Experiment (SEE) on the TIMED spacecraft has been providing solar spectral irradiance products since January 2002 [*Woods et al.*, 2000]. This data set contains daily averaged spectral irradiance from 0.5 to 190 nm. These data provide a check on the SORCE data but only in the FUV band. They are shown in red in Figure 1.

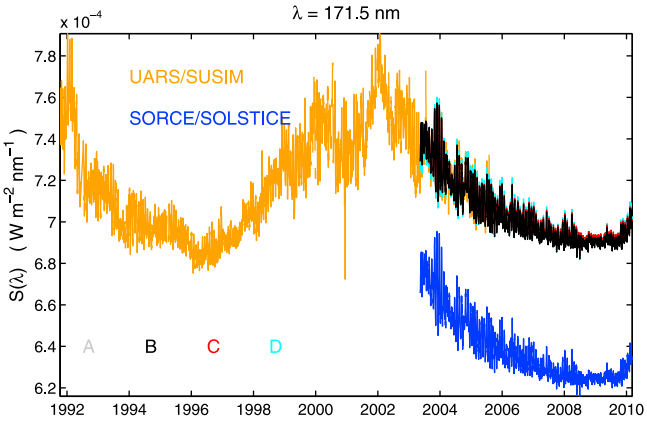

Figure 2. Example correlations for a 1 nm band around λ = 171.5 nm., with raw UARS/SUSIM data (orange) and SORCE/SOLSTICE data (blue). Composite data series for methods A, B, C and D applied to the SORCE data are shown in gray, black, red and cyan, respectively.

[11] Figure 1 shows that, at the time of writing at least, the only available data that covers all of the "SOLSTICE gap" (between the end of available UARS/SOLSTICE data and the start of the SORCE/SOLSTICE data) comes from the SUSIM instrument: the SUSIM data are therefore unique for producing a data composite that covers both the 1996 and the 2009 minima, if one wants to avoid using proxies such as Mgii. This situation may improve as work continues to extend the UARS/SOLSTICE data analysis into the period covered by SORCE. However, there are problems with data from both UARS instruments in later years. Both the SUSIM and SOLSTICE data were affected by the failure of a tape drive in October 1999 and of a star tracker in 2002. These failures have limited the in-flight calibration possibilities and so may have introduced calibration drifts as well as discrete skips. In the present paper we consider the possible use of SUSIM as a way of combining the SORCE and UARS/SOLSTICE data sets as an alternative to the use of a proxy-based model.

3. Analysis

[12] Figure 1 demonstrates the various data series. To achieve intercalibration between UARS/SUSIM data and the SORCE data, we employ the overlap period of 2.22 years between May 2003 and August 2005 and intercalibrate the data for each 1 nm wide wavelength band independently. We carry out the intercalibration in four different ways (which we here term methods A, B, C and D), which are described in sections 3.1 to 3.4. Initially these methods are applied assuming that the SUSIM data are accurate and applying the adjustment to the SORCE data to extend the SUSIM data to 2010 (section 4.1). Subsequently, the SORCE data are assumed to be correct and same four methods are used to apply adjustments to the SUSIM data to extrapolate them back to the interval also covered by UARS/SOLSTICE and the adjusted SUSIM data are the calibrated with the UARS/SOLSTICE data (section 4.2). The methods are only applied at wavelengths where various correlations meet certain criteria discussed later. Figure 2 presents an example of the results from the four methods when applied to the SORCE data, for an example wavelength of λ = 171.5 nm. In this plot, the orange variation is the SUSIM data, the blue line is the uncalibrated SORCE data (at this wavelength, from the SOLSTICE instrument). The results for methods A, B, C and D and are shown in gray, black, red and cyan, respectively. (Note that the differences are so small that these results are often indistinguishable in this plot). Figure 3 shows the period of data overlap in more detail. The upper panel shows the same data as Figure 2 on an expanded timebase and reveals the strong 27 day oscillation caused by solar rotation. In many places the differences between the curves is smaller than the linewidth. To reveal the differences in more detail, the lower panel of Figure 3 shows the deviation ΔS of the various adjusted SORCE data from the SUSIM data, where $\Delta S = S_{SUSIM} - f_X(S_{SORCE})$, and $f_X(S_{SORCE})$ is the adjusted SORCE data using method X (discussed below). The blue line shows the linear fit to the values for method B (in black) and illustrates the upward trend of the fit residuals.

3.1. Method A

[13] This method was one of those employed by *Lockwood et al.* [2010b] and assumes that there is only a systematic zero-level offset between UARS/SUSIM and the SORCE data. A zero-level offset c is introduced and varied until the minimum r.m.s. deviation of the SUSIM and corrected SORCE data is found. The adjusted SORCE data are given by $f_A(S_{SORCE}) = S_{SORCE} + c$. The same offset c is then applied to all the SORCE data so the sensitivity and zero-level offset of the SORCE instrument is assumed to be constant with time, i.e., that all instrument degradations has been correctly allowed for in the data processing of both data sets and only a systematic offset needs correcting. The variations are shown in gray in Figures 2 and 3.

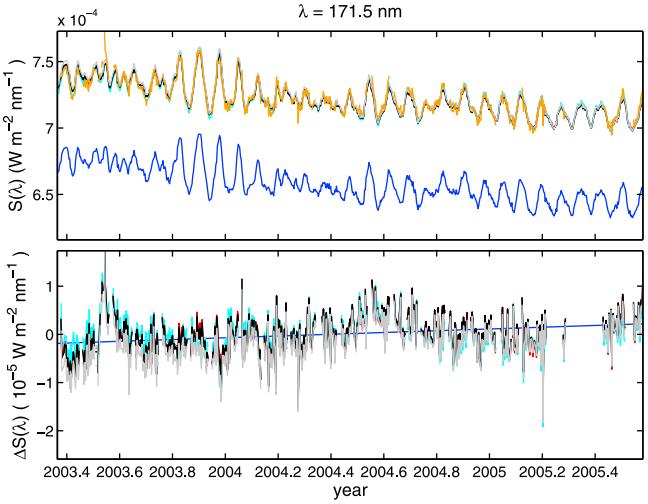

Figure 3. (top) Detail of Figure 2 for the overlap interval when both SUSIM and SORCE data are available. (bottom) The deviations of the various composite series from the SUSIM data, using the same color scheme as in the top panel and in Figure 2. The blue line is the linear fit to the deviations for method B and illustrates the upward trend in the fit residuals.

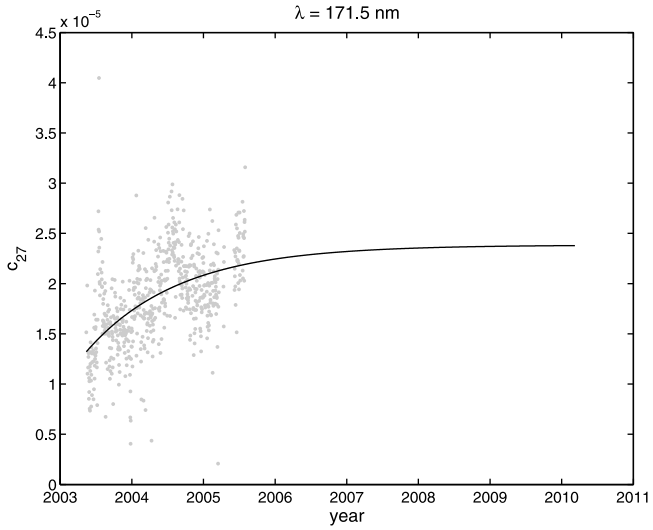

Figure 4. The form of the time-dependent offset used in correlation method D, c_{27}. Grey dots show the daily values needed for the overlap period, and the line is the best fit curve using an exponential decay.

3.2. Method B

[14] This method was the other one employed by *Lockwood et al.* [2010b]. It is assumed that both instrument sensitivity and zero-level offset need correcting but, again, neither vary with time. A linear regression of the simultaneous daily data is taken and the SORCE data adjusted for both the best fit slope s and intercept c. The adjusted SORCE data are $f_B(S_{SORCE}) = s \times S_{SORCE} + c$. The result is the black line in Figures 2 and 3.

3.3. Method C

[15] This method aims to match the long-term trends without the influence of the 27 day variation. The method makes the same assumptions as method B but the intercalibration regression is carried out on 27 day running means of the data, as opposed to daily values, giving slope s_m and intercept c_m so that $f_C(S_{SORCE}) = s_m \times S_{SORCE} + c_m$. The result is the red lines in Figures 2 and 3 which are again very similar to the results of methods B and A, such that the difference can only be seen for a few data points at this wavelength.

3.4. Method D

[16] This method uses the amplitude of the 27 day oscillations. The SUSIM and SORCE data are detrended using the 27 day running means and the sensitivity factor for the two instruments found by taking the slope, s_{27}, of the regression of the detrended values. By detrending the data, information on the zero-level offset is lost. For this method we do not assume the zero-level offset is constant. It is found that the best fit is an exponential for most wavelengths (although the fitted exponent is so large in several cases that it is very close to linear). The calibrated data is therefore $f_D(S_{SORCE}) = s_{27} \times S_{SORCE} + c_{27}(t)$. The offset required is evaluated for each daily value, as shown by the gray dots in Figure 4 for the same example presented in Figures 2 and 3 (λ = 171.5 nm). The solid line is the best least squares fit exponential decay of this offset, fitted using the Nelder-Mead search method. The fitted offsets are then added to the scaled detrended data to generate the cyan variations shown in Figures 2 and 3, which again are very similar indeed to the SUSIM data and the results from the other methods at this wavelength.

[17] It was also investigated if an exponential decay in the sensitivity factor would help to fit the two data sets. This was done by carrying out linear regressions for individual 27 day solar rotations and then fitting an exponentially decaying functional form to the variation of derived sensitivity and offset factors. In many cases, no improvement was made to the fits and the results were very similar to those obtained by methods A–D. At some wavelengths, however, this procedure was unstable and generated a radically different result, but one which we could discount because applying it to the whole of the SORCE data series shifted the time of the recent minimum appreciably (by more than 1 year). Thus we found no consistent evidence for a varying sensitivity factor (beyond the corrections already made in the analysis of the raw SSI data).

4. Results

4.1. Assuming the SUSIM Data Are Correct

[18] Figure 5 shows the correlations obtained from the data overlap period for the data shown in Figure 3. The top panel shows r_B, the correlation between the daily SUSIM and SORCE data (on which calibration method B is based), as a function of wavelength. The plot extends up to λ = 320 nm, which means all the SORCE data were supplied by the SOLSTICE instruments on board that satellite. The analysis was also carried out at all λ up to 400 nm using data from the SIM instrument (not shown), but r_B was lower and hence we restricted the range of λ studied. The second panel in Figure 5 shows the correlation r_C between 27 day running means of the SUSIM and SORCE data (on which method C is based) and the third panel shows the correlation r_D between the detrended 27 day oscillations (on which method D is based). We here require that all of r_B, r_C and r_D exceed 0.8 for the SORCE and SUSIM data to be considered sufficiently similar that any intercalibration between the two might be valid. The choice of the 0.8 threshold is arbitrary, but Figure 5 shows that the distributions of correlation coefficients above and below this threshold are distinct for r_B and r_D. The 0.8 thresholds are shown by horizontal dashed lines in the top three panels of Figure 5, and correlations which exceed this level are highlighted with a solid circle. Note that the 27 day smoothing gives r_C values which generally exceed r_B and r_D and that, in general, r_B values exceed r_D. There is a band of wavelengths between 150 and 210 nm where the raw, smoothed and detrended variations from SUSIM and SORCE all correlate highly. Thus we restrict our attention to this band as we have most confidence here that SORCE can provide a valuable composite data series when combined with UARS/SOLSTICE, using SUSIM to intercalibrate across the gap. Note that outside this band correlations can be weaker because of problems with the SUSIM data or the SORCE data, or both.

[19] To summarize the results we here integrate the data into 10 nm bands. The fourth panel of Figure 5 shows N, the

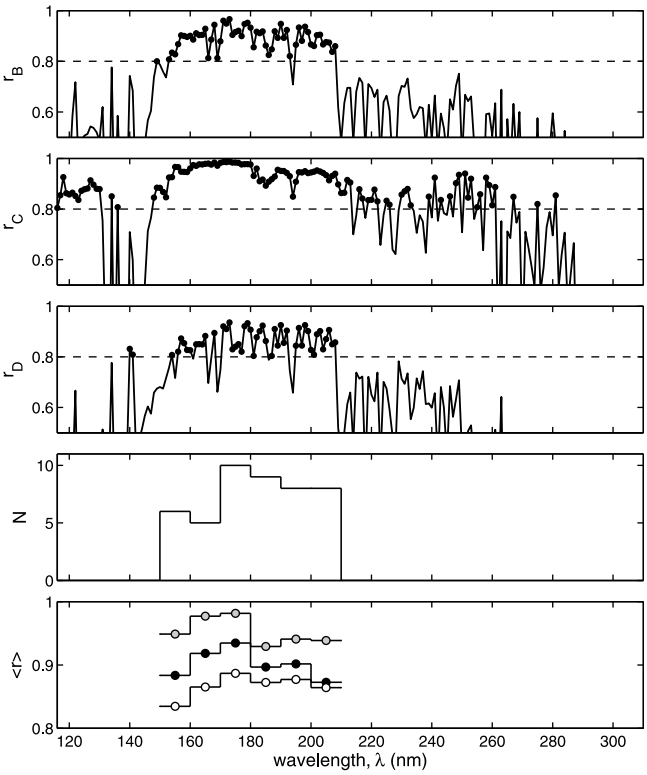

Figure 5. (top to bottom) Correlations for daily, 27 day running mean and detrended daily data (r_B, r_C and r_D, respectively) as a function of wavelength, λ. Correlation coefficients exceeding the required 0.8 level (horizontal dashed line) are shown by dots. The number of 1 nm time series, N within 10 nm bands for which $r_B > 0.8$, $r_C > 0.8$ and $r_D > 0.8$. The bottom panel shows the mean of the correlations for the N time series used in the 10 nm bands: solid circles are $\langle r_B \rangle$, gray circles are $\langle r_C \rangle$ and open circles are $\langle r_D \rangle$.

number of wavelengths in 10 nm bands for which $r_B > 0.8$, $r_C > 0.8$ and $r_D > 0.8$. The bottom panel shows the averages of r_B, r_C and r_D for the N usable data sequences in those 10 nm bands. Figure 6 shows the mean variations for the N wavelengths in each band obtained by assuming the SUSIM data are correct and adjusting the SORCE data by methods B (in black) and A (in mauve). The blue curves show the corresponding average variation of the unadjusted SORCE data for the same set on N wavelengths. The green lines show the corresponding band means for UARS/SOLSTICE data. These have been intercalibrated with the SUSIM data by method A (offset only) for the interval 1999–2001. Also in each panel, the 27 day running mean of the variation obtained by method B is shown in yellow. The minimum in the 27 day means in the intercalibrated UARS/SOLSTICE data between solar cycles 22 and 23, S_{m1}, is marked by a horizontal dashed line in each panel.

[20] Figure 6 does not present definitive time series composites, but it does give some idea of how the variously adjusted data compare to the unadjusted data. It can be seen that for λ range of 150–160 nm, the minimum value of the 27 day means between cycles 23 and 24, S_{m2}, is slightly higher than its predecessor for both methods A and B, i.e., $\delta_{min} = (S_{m2} - S_{m1}) > 0$. This difference is even more marked for 160–170 nm, for which δ_{min} again is positive. For 170–180 nm, method A gives a considerably lower second minimum ($\delta_{min} < 0$) whereas method B gives a slightly lower one. Both methods agree that for 180–190 nm the two minima are very similar ($\delta_{min} \approx 0$) and that for 190–200 nm the second minimum is very slightly lower than the first ($\delta_{min} < 0$). This negative δ_{min} is considerably more pronounced for 200–210 nm, particularly for method A. Note that the y axis scales in Figure 6 vary from band to band because of the shape of the UV spectrum. Table 1 compares the results of all for methods. To allow comparison of the wavelength bands, the values of δ_{min} are given as a percentage of S_{m1}. The table also gives the solar cycle amplitude $A = (S_{max} - S_{m1})$ from the intercalibrated

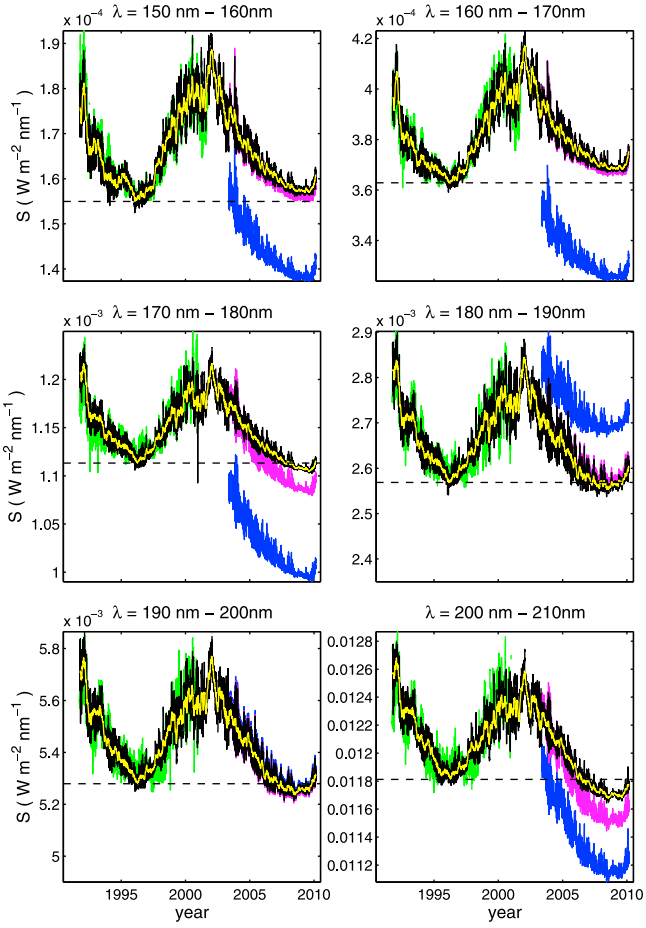

Figure 6. Composite time series for the six 10 nm bands in which $N \geq 5$. Black shows the corrected variation for method B, S_B, the 27 day running means of which, $\langle S_B \rangle_{27}$, are shown in yellow. The horizontal dashed line is the minimum of $\langle S_B \rangle_{27}$ for the minimum between cycles 22 and 23. The raw published SORCE/SOLSTICE data are shown in blue, and data adjusted by method A (zero-level adjustment only) are shown in mauve. The best fit UARS/SOLSTICE data (using method A) are shown in green. Note that these variations rely on the SUSIM data being accurate and are included here as illustrations of the procedure used rather than as the definitive composite variations.

Table 1. Percent Changes in Solar Spectral Irradiance $S(\lambda)$, Derived According to the Assumption that the SUSIM Data are Correct in the Overlap Period[a]

λ Band (nm)	Minimum S Between Cycles 22 and 23, S_{m1}(W m^{-2} nm^{-1})	Percent Solar Cycle Amplitude, $100A/S_{m1}$	Percent Change Between Minima, $100\delta_{min}/S_{m1}$				
			For Raw SORCE Data	Calibration Method			
				A	B	C	D
150–160	1.550×10^{-4}	21.72	−11.02	0.34	1.30	2.01	1.25
160–170	3.629×10^{-4}	14.96	−10.37	1.06	1.46	1.37	1.39
170–180	1.113×10^{-3}	9.27	−10.73	−2.71	−0.74	−0.56	−0.49
180–190	2.569×10^{-3}	10.72	4.46	−0.01	−0.60	−1.49	−0.91
190–200	5.280×10^{-3}	9.28	−0.66	−0.96	−0.81	−0.56	−0.71
200–210	1.181×10^{-2}	6.57	−5.83	−2.71	−1.15	−0.60	−1.00

[a]δ_{min} is the difference between the solar minimum 22/23 (S_{m1} in 27 day running means) and that for solar minimum 23/24 (S_{m2}), i.e., $\delta_{min} = (S_{m2} - S_{m1})$. Column 3 gives the percent solar cycle amplitude: $A = (S_{max} - S_{m1})$, where S_{max} is the peak 27 day mean of solar cycle 23.

UARS/SOLSTICE and SUSIM data, where S_{max} is the peak 27 day mean of solar cycle 23: again A is expressed as a percentage of S_{m1}. Table 1 also gives the values for $100\delta_{min}/S_{m1}$ obtained if the SORCE data are used without any intercalibration with SUSIM. All calibration methods give a smaller change δ_{min} between the two minima than do the unadjusted SORCE data.

[21] The ratio δ_{min}/A was also computed for each 1 nm wavelength band individually (for which $r_B > 0.8$, $r_C > 0.8$ and $r_D > 0.8$) and using all four calibration methods. The results are shown in the top panel of Figure 7: solid gray circles, solid black circles, open triangles and solid gray diamonds show the results for calibration methods A, B, C and D, respectively. The general trend noted in Figure 6 and Table 1 is seen for all calibration methods, in that for shorter wavelengths ($\lambda < 175$ nm), δ_{min}/A is consistently positive whereas it is consistently negative for $\lambda > 185$ nm.

[22] The second panel of Figure 7 shows the correlation coefficients of the SUSIM data with the SORCE data after the various intercalibrations (using the same symbols as in the top panel). It can be seen that the calibration method makes very little difference to the correlation. However, in terms of evaluating any change between the two minima it is important to look at the trends in the fit residuals. The points in the four panels of Figure 8 show the residuals $\Delta S = S_{SUSIM} - f_X(S_{SORCE})$, where f_X is the calibration function, as a function of time, t. This plot is for the same example wavelength ($\lambda = 171.5$ nm) as Figures 2, 3 and 4. Also shown in each case is the least squares linear regression fit of slope $S_r = d\Delta S/dt$. The ideal fit would have $S_r = 0$, as then no drift between the SUSIM data and the adjusted SORCE data would have been detected over the period of overlapping data. In the example shown in Figure 8, $S_r > 0$ for calibration methods A, B and C: this shows that the calibrated SORCE estimates $f_X(S_{SORCE})$ are increasingly too small, and hence implies that using these $f_X(S_{SORCE})$ to extrapolate to the minimum between cycles 23 and 24 is likely to lead to an S_{m2} value that is too low and hence a δ_{min} estimate that is too low (in the case of negative δ_{min}, meaning $|\delta_{min}|$ is too large). Method D does yield a much lower value of $|S_r|$ because a time-varying offset is fitted. Figure 7c shows the values of (S_r/A) as a function of wavelength, using the same symbols as in Figures 7a and 7b. Figure 7d shows the estimates of δ_{min} with a correction of $y \times S_r$ made to allow for the drift in the residuals over the $y = 2.95$ yrs between the end of the SUSIM data and the second solar minimum. The correction allows for a linear drift in the offset, and Figure 7d shows that after this correction for the drift, methods A, B and C all give almost identical estimates of the variation between the minima. Method D, with correction, gives almost identical results to the other three at λ below about 190 nm.

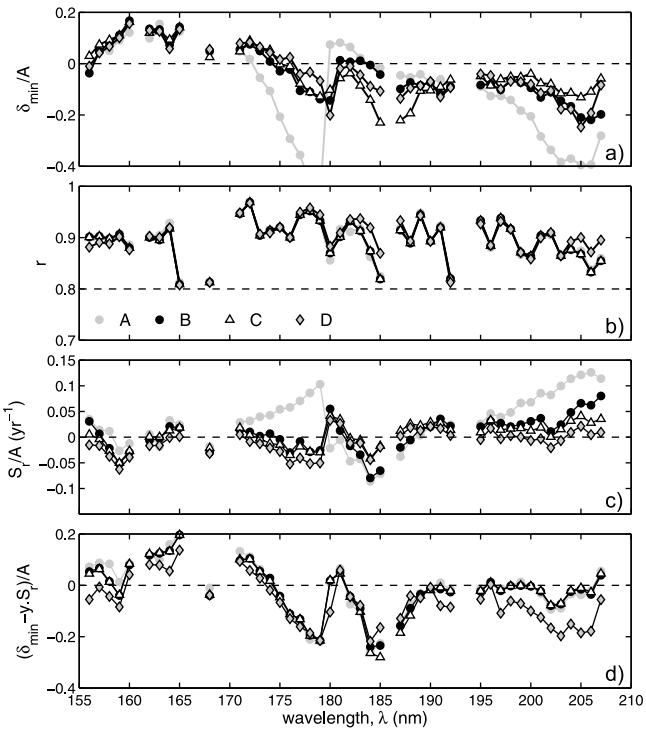

Figure 7. (a) Fractional changes in solar minimum spectral irradiance $S(\lambda)$ for 1 nm wavelength intervals. $\delta_{min} = (S_{m1} - S_{m2})$ is the difference between the minimum 27 day running mean for solar minimum 22/23 (S_{m1}) and that for solar minimum 23/24 (S_{m2}); it is shown as a fraction of A, the solar cycle amplitude ($A = S_{max} - S_{m1}$, where S_{max} is the 27 day running mean peak of cycle 23). (b) The correlation coefficients, r. (c) Fractional change per year in the overlap interval, S_r/A, where S_r is the temporal gradient in the fit residuals (i.e., $S_r = d\Delta S/dt$). (d) The same as panel (b), corrected for the drift residuals $(\delta_{min} - y\ S_r)/A$. In all panels, solid gray circles, solid black circles, open triangles and solid gray diamonds represent calibration methods A, B, C and D, respectively.

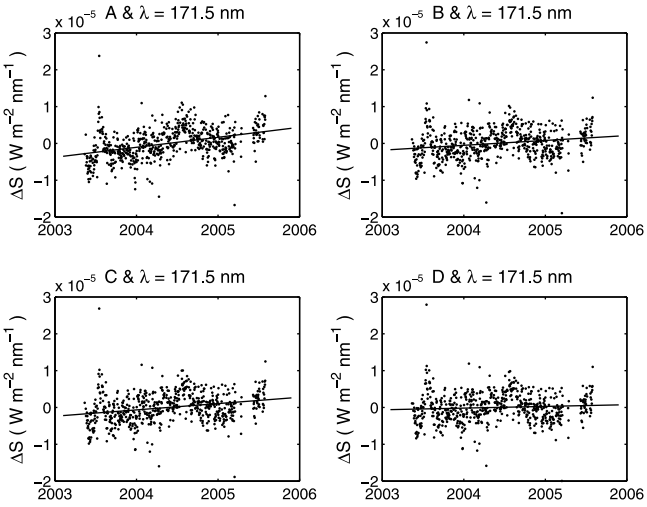

Figure 8. Fit residuals, ΔS, as a function of time, where ΔS is defined as the UARS/SUSIM data minus the best fit SORCE data, $\Delta S = S_{SUSIM} - f_X(S_{SORCE})$. Each of the four panels shows one method of SORCE calibration, A, B, C or D. The solid lines are the best fit linear regression lines which have slope S_r.

However, at wavelengths longer than this a lower second solar minimum (giving negative δ_{min}/A) persists for method D. Given that the correction for the drift in the fit residuals is equivalent to adding a time-dependent (linearly varying) offset, the negative values for method D at $\lambda > 190$ nm arise only because of the use of an exponentially varying offset.

[23] Hence, in summary, all methods agree that (δ_{min}/A) is positive at λ between 155 nm and 175 nm (Figure 7a). The fit residuals are low (Figure 7c) and correcting for them with a linear variation does not alter this (Figure 7d). The positive value means that the recent minimum is less deep than its predecessor. At 175–181 nm there are negative values of (δ_{min}/A) (i.e., the recent minimum is deeper than its predecessor) that are similarly seen using all methods and values become slightly more negative if the drifts in the residuals are allowed for. There are suggestions of a second band of negative (δ_{min}/A) at 183–190 nm. All of the above results are relatively clear-cut. The situation at $\lambda > 195$ nm is less clear. In this range, all methods yield negative (δ_{min}/A). However, inspection of Figure 7c shows that (S_r/A) is positive here, and the derived negative (δ_{min}/A) values are roughly equal to the derived (yS_r/A), which means that, allowing for the drift in the residuals, we find no consistent change in the minima for the wavelength band of usable correlations at $\lambda > 195$ nm.

4.2. Assuming the SORCE Data Are Correct

[24] In subsection 4.1 the correlations and linear regressions were used to adjust the SORCE data and use these adjusted data to extend the UARS SUSIM data sequence to the recent solar minimum. In this subsection, the SORCE data are taken to be correct and the SUSIM data adjusted by methods A, B, C, and D so that they can be used to extend the sequence back to the interval also covered by the UARS/SOLSTICE data. The adjusted SUSIM data are then matched to the last 2 years of UARS/SOLSTICE data using method A to generate a composite. The composite data series at each wavelength obtained this way is then smoothed with a 27 day running mean, as in the previous subsection and (δ_{min}/A) computed for each 1 nm wavelength band for which $r_B > 0.8$, $r_C > 0.8$ and $r_D > 0.8$). Table 2 compares the results of all four methods and corresponds to Table 1. In this case the comparison of the wavelength bands is made possible by expressing δ_{min} as a percentage of S_{m2} (as in this case S_{m2} rather than S_{m1} does not depend on the intercalibration method used). The solar cycle amplitude $A = (S_{max} - S_{m1})$, where S_{max} and S_{m1} are taken from the combined data from the two UARS instruments, and in Table 1 A is expressed as a percentage of S_{m2}. Table 2 also gives the values for $100\delta_{min}/S_{m2}$ obtained if the UARS/SOLSTICE data are used without any intercalibration with SORCE. Like Table 1, Table 2 shows that the calibration methods give a smaller change δ_{min} between the two minima than do the unadjusted UARS data (the only exception to this is method D for λ = 200–210 nm, which gives a similar value to the unadjusted data).

[25] As in subsection 4.1, the drift in the residuals (now defined as $\Delta S = S_{SORCE} - f_X(S_{SUSIM})$, i.e., the SORCE data minus the best fit-adjusted UARS/SUSIM data) is evaluated and corrected for. The period of overlap between SUSIM and SORCE starts at 2003.4, and the adjusted SUSIM data are compared with the UARS SOLSTICE data (via method A) over the interval 1999–2001: taking the middle of this interval, the adjusted SUSIM data are effectively an extrapolation over $y = 3.4$ years, and this is the value used to correct for the residual drift to give $(\delta_{min} - y \times S_R)/A$.

[26] The results are shown in Figure 9, which corresponds to Figure 7. The same pattern of UV spectral change between the two minima emerges. Method D is much more

Table 2. Percent Changes in Dolar Spectral Irradiance $S(\lambda)$, Derived According to the Assumption that the SORCE Data are Correct in the Overlap Period

λ Band (nm)	Minimum S Between Cycles 23 and 24, S_{m2}(W m^{-2} nm^{-1})	Percent Solar Cycle Amplitude, $100A/S_{m2}$	Percent Change Between Minima, $100\delta_{min}/S_{m2}$				
			For Raw UARS-SOLSTICE Data	Calibration Method			
				A	B	C	D
150–160	1.539×10^{-4}	21.41	−11.01	−1.79	−1.93	−2.43	−4.88
160–170	2.692×10^{-4}	19.34	−13.98	0.98	0.97	1.06	−0.09
170–180	9.935×10^{-4}	12.20	−12.02	−1.88	−2.39	−2.48	−4.67
180–190	2.708×10^{-3}	10.67	4.23	−0.03	0.02	−0.37	1.26
190–200	5.558×10^{-3}	9.83	−0.63	−0.12	−0.50	−0.62	−1.80
200–210	9.530×10^{-3}	8.40	−7.22	−2.13	−2.83	−3.16	−5.84

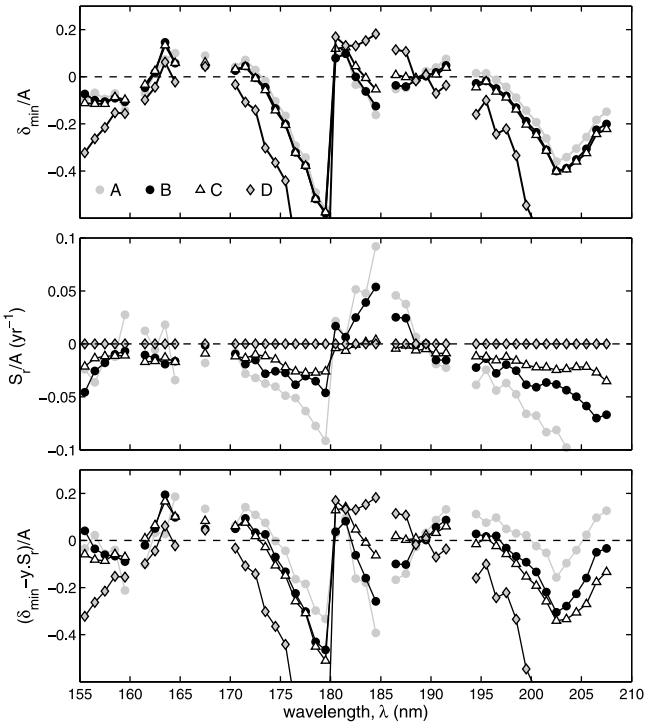

Figure 9. Variations of (δ_{min}/A), S_R/A and $(\delta_{min} - y \times S_R)/A$ with wavelength λ for methods A (gray circles), B (solid black circles), C (open triangles) and D (solid gray diamonds), applied with the assumption that the SORCE data are correct.

variable due to the use of the exponential form. This is because in the previous section we were adjusting the SORCE data for after the overlap period, whereas here we are adjusting the SUSIM data for before the overlap period. That places us on the larger-gradient part of the exponential curve, and this additional sensitivity is reflected in Figure 9. The variations in (δ_{min}/A) are similar to those in Figure 7, but all are shifted to lower values. This means that the positive values seen at $\lambda < 170$ nm are smaller than for the previous intercalibration (compare Figures 7 and 9). However, it also means that the negative values seen at $175 < \lambda < 181$ nm and at $\lambda > 195$ nm are of greater magnitude than before. Unsurprisingly, the drift in the fit residuals for method A is high, but methods B and C still show strong negative values after the residual drift is corrected for. The variable offset of method D has removed the drift in the residuals completely.

5. Discussion

[27] We have investigated using four methods to employ the UARS SUSIM data to bridge the "SOLSTICE gap" between the end of the UARS SOLSTICE data and the start of the SORCE SOLSTICE data and thereby ensure the data sequence in UV spectral irradiance is homogeneous. In addition, we have assumed SUSIM is correct and adjusted SORCE/SOLSTICE data and vice versa. The correlations are good at wavelengths up to about 200 nm.

[28] A drift in the fit residuals ($S_r \neq 0$), as illustrated in Figure 8, means that there is drift within the overlap period in one data sequence relative to the other, even after the mean intercalibration for the whole period has been applied (by one of the methods A–D). Only Method D allows for such a drift because it fits a time-varying offset value. (Note, however, that because this is slowly varying, sudden jumps in either data sequence are still not allowed for.) Method D uses an exponentially varying offset, which can be seen to be effective because S_r for this method is always small. Once corrected for the drift in the residuals, methods A, B and C have allowed for a linear drift in the offset.

[29] The variations of (δ_{min}/A) shown in Figures 7 and 9 are quite similar, and in all cases the changes depend on λ: this is true if SUSIM is assumed to be correct and the SORCE data fitted to it, or vice versa. Thus we have evidence for a change in the shape of the UV spectrum between the two minima.

[30] The main difference between the two sets of results is that assuming SORCE/SOLSTICE is correct and adjusting SUSIM data across the "SOLSTICE gap" produces generally lower values for the recent solar minimum than for its predecessors than does the alternative procedure (i.e., assuming SUSIM data are correct and adjusting the SORCE data up to the recent solar minimum). Of the two approaches, assuming that SORCE data are correct is preferable, given that the SORCE data have higher levels of in-flight calibration available and SUSIM has a number of known uncertainties. Early degradation of the SORCE instrument may have been faster than it was later in the overlap period and may have been inadequately compensated for (this would explain the success of the exponential form in method D), but to some extent this would also be allowed for by the linear correction for the drift residuals.

[31] Figure 10 plots sunspot minima and sunspot maximum spectra. These are integrations over 1 year intervals: $S_{m1}(\lambda)$ is the spectrum during the first sunspot minimum, integrated over the interval 1995.5–1996.5 (in red); $S_{m2}(\lambda)$ is the spectrum during the second sunspot minimum, integrated over the interval 2008.5–2009.5 (in black); $S_{max}(\lambda)$ is the spectrum during the intervening sunspot maximum, integrated over the interval 2000–2001 (in blue). The left-hand panel shows the SOLSTICE data (S_{m1} being from UARS and S_{m2} being from SORCE) with no calibration adjustments applied. The right-hand panel shows the results of applying method D and assuming that SORCE is correct. The two plots have differences but are similar in general. This means that applying method D (applying an exponentially decaying offset drift to the SUSIM data) makes the data from SOLSTICE instruments on UARS and SORCE consistent at most wavelengths, and such a drift would mean that at the larger wavelengths where comparison is possible (195–205 nm), the decline in the solar minimum irradiance is real.

[32] *Rozanov et al.* [2002] have studied the effects of different UV wavelengths on stratospheric temperature and ozone abundance. The highest sensitivity to the solar flux variations is in the spectral bands 195–215 nm (the Herzberg oxygen continuum) and 260–290 nm (the Hartley ozone band). Because the oxygen cross sections are not so large in the Herzberg continuum, the solar signal at 195–215 nm can be detected even in the lower stratosphere. In the upper stratosphere and mesosphere the ozone and temperature are the most sensitive to the solar flux variability in Lyman α

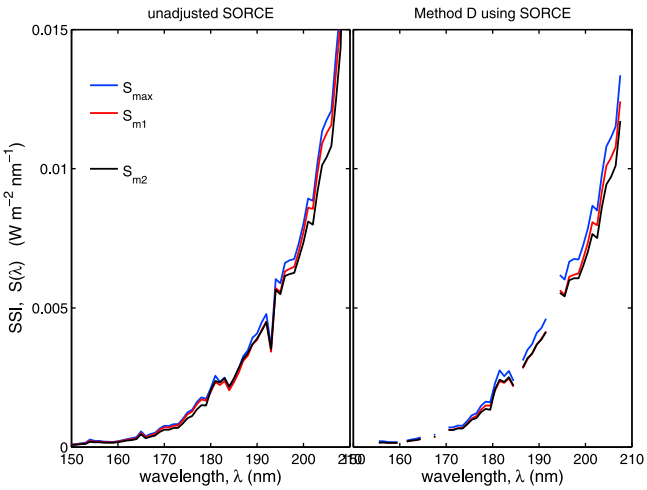

Figure 10. Integrated spectra over 1 year intervals at sunspot minimum and sunspot maximum. $S_{m1}(\lambda)$ is the spectrum during the first sunspot minimum, integrated over the interval 1995.5–1996.5 (in red); $S_{m2}(\lambda)$ is the spectrum during the second sunspot minimum, integrated over the interval 2008.5–2009.5 (in black); $S_{max}(\lambda)$ is the spectrum during the intervening sunspot maximum, integrated over the interval 2000–2001 (in blue). (left) The SOLSTICE data (S_{m1} being from UARS, and S_{m2} being from SORCE) with no calibration adjustments applied. (right) The results of applying intercalibration method D while assuming that the SORCE data are correct.

line (121.6 nm) and Schumann-Runge bands (180–200 nm). These authors conclude that wavelengths around 210 nm are mostly responsible for the temperature and ozone response in the relatively dense lower stratosphere. The second important spectral band is Hartley ozone absorption band centered at 270 nm. Calibrations that we can be confident of in this paper (correlation coefficients for daily, 27 day smoothed and detrended data all exceeding 0.8) extend only up to 210 nm.

[33] *Lockwood et al.* [2010b] studied the variations throughout the UV band using methods A and B to intercalibrate the SORCE data. They found that method A give a large decline in MUV (200–270 nm) between the two minima but a smaller decline for method B, consistent with the findings for 195–208 nm reported here. The present study supports their view that the results of method B are the more realistic. These authors also studied the FUV band (120–200 nm) and found only a small difference between the minima by both methods. The results presented here show an increase (or no change) at shorter wavelengths and a decrease at longer wavelengths in this FUV band, and so averaging over the band may have disguised some of the changes.

[34] From the above, we conclude that there is evidence for a change in the minima at FUV wavelengths; however, its magnitude depends on the method used to intercalibrate the data. The more favored option (assuming the SORCE data to be correct) does yield significantly lower values during the recent solar minimum than during the previous minimum over much of the wavelength range studied. If method D is used to correct the SUSIM data, it gives no drift in the fit residuals and shows that applying an exponentially decaying offset in the SUSIM data makes it broadly consistent with the unadjusted UARS and SORCE SOLSTICE data sets. A difference between these two minima at $\lambda > 195$ nm is significant for understanding some effects of long-term solar variability on climate, given that this would be evidence or a decline in the solar minimum UV spectral irradiance at the wavelengths responsible for stratospheric ozone production and heating. However, the results also place limits on the solar changes. Several studies show that the present minimum is a return to conditions last seen in about 1920 [*Lockwood et al.*, 2009b; *Lockwood*, 2010] and from Figure 10, the change appears to be between about 20% and 100% (depending on wavelength) of the amplitude of recent solar cycle variations in the wavelength range 195–205 nm.

6. Conclusions

[35] The SUSIM and SORCE UV spectral irradiances are sufficiently similar during the interval when they are both available (May 2003 to August 2005) that an attempt can be made to intercalibrate them for the wavelength range 156–208 nm. We have used four different calibration methods, all of which indicate a change in the shape of the spectrum of solar UV emission between the solar cycle minimum between cycles 22 and 23 (at which $S = S_{m1}$) and the most recent minimum (at which $S = S_{m2}$).

[36] The high correlations in the wavelength band studied ensure that the results obtained by assuming that the SUSIM data are correct (and adjusting SORCE) are not so greatly different from those obtained by assuming SORCE is correct (and adjusting SUSIM).

[37] All calibrations give composites with $S_{m2} \geq S_{m1}$ at much of the band $\lambda < 175$ nm but there are indications that $S_{m1} > S_{m2}$ at $\lambda > 195$ nm where UV is most effective in generating ozone and heating the stratosphere [*Rozanov et al.*, 2002]. This is particularly true if the SORCE data are assumed to be correct and the standard by which to correct the SUSIM data in the SOLSTICE gap.

[38] Last, an important caveat must be placed on these results. Any spurious step-function change in the SUSIM data during the SOLSTICE gap will be reflected in the derived changes between the minima, whatever calibration method is used. There are three possibilities available to investigate this. One is processing of any UARS/SOLSTICE data that can be recovered during the SOLSTICE gap. However, because some issues on UARS (e.g., spacecraft pointing accuracy) will influence both instruments, this may not always be an independent test. A second possibility at some wavelengths is to use SEE data, but sampling rate and noise level differences would have to be allowed for. The third possibility is that proxy series are used to check for sudden discontinuities, but this would not be an adequate test of gradual calibration drifts.

References

Abreu, J. A., J. Beer, F. Steinhilber, S. M. Tobias, and N. O. Weiss (2008), For how long will the current grand maximum of solar activity persist?, *Geophys. Res. Lett.*, *35*, L20109, doi:10.1029/2008GL035442.

Baldwin, M. P., and T. J. Dunkerton (1999), Propagation of the Arctic Oscillation from the stratosphere to the troposphere, *J. Geophys. Res.*, *104*(D24), 30,937–30,946, doi:10.1029/1999JD900445.

Brohan, P., J. J. Kennedy, I. Harris, S. F. B. Tett, and P. D. Jones (2006), Uncertainty estimates in regional and global observed temperature

changes: A new data set from 1850, *J. Geophys. Res.*, *111*, D12106, doi:10.1029/2005JD006548.

Brueckner, G. E., K. L. Edlow, L. E. Floyd IV, J. L. Lean, and M. E. VanHoosier (1993), The Solar Ultraviolet Spectral Irradiance Monitor (SUSIM) Experiment on board the Upper Atmosphere Research Satellite (UARS), *J. Geophys. Res.*, *98*(D6), 10,695–10,711, doi:10.1029/93JD00410.

DeLand, M. T., and R. P. Cebula (2008), Creation of a composite solar ultraviolet irradiance data set, *J. Geophys. Res.*, *113*, A11103, doi:10.1029/2008JA013401.

Dewitte, S., D. Crommelynck, S. Mekaoui, and A. Joukoff (2004), Measurement and uncertainty of the long-term total solar irradiance trend, *Sol. Phys.*, *224*, 209–216, doi:10.1007/s11207-005-5698-7.

Dudok de Wit, T., M. Kretzschmar, J. Lilensten, and T. Woods (2009), Finding the best proxies for the solar UV irradiance, *Geophys. Res. Lett.*, *36*, L10107, doi:10.1029/2009GL037825.

Fröhlich, C. (2006), Solar irradiance variability since 1978: Revision of the PMOD composite during solar cycle 21, *Space Sci. Rev.*, *125*(1–4), 53–65, doi:10.1007/s11214-006-9046-5.

Fröhlich, C. (2009), Evidence of a long-term trend in total solar irradiance, *Astron. Astrophys.*, *501*(3), L27–L30, doi:10.1051/0004-6361/200912318.

Gray, L. J., S. Crooks, C. Pascoe, S. Sparrow, and M. Palmer (2004), Solar and QBO influences on the timing of stratospheric sudden warmings, *J. Atmos. Sci.*, *61*, 2777–2796, doi:10.1175/JAS-3297.1.

Gray, L. J., et al. (2010), Solar influences on climate, *Rev. Geophys.*, *48*, RG4001, doi:10.1029/2009RG000282.

Haigh, J. D. (2003), The effects of solar variability on the Earth's climate, *Philos. Trans. R. Soc. A*, *361*, 95–111, doi:10.1098/rsta.2002.1111.

Haigh, J. D., A. R. Winning, R. Toumi, and J. W. Harder (2010), An influence of solar spectral variations on radiative forcing of climate, *Nature*, *467*, 696–699, doi:10.1038/nature09426.

Hansen, J., R. Ruedy, J. Glascoe, and M. Sato (1999), GISS analysis of surface temperature change, *J. Geophys. Res.*, *104*(D24), 30,997–31,022, doi:10.1029/1999JD900835.

Harder, J. W., J. M. Fontenla, P. Pilewskie, E. C. Richard, and T. N. Woods (2009), Trends in solar spectral irradiance variability in the visible and infrared, *Geophys. Res. Lett.*, *36*, L07801, doi:10.1029/2008GL036797.

Harder, J. W., G. M. Lawrence, G. J. Rottman, and T. N. Woods (2000), The Spectral Irradiance Monitor (SIM) for the SORCE mission, *Proc. SPIE Int. Soc. Opt. Eng.*, *4135*, 204–214, doi:10.1117/12.494225.

Harder, J., et al. (2005a), The Spectral Irradiance Monitor: Scientific requirements, instrument design, and operation modes, *Sol. Phys.*, *230*(1–2), 141–167, doi:10.1007/s11207-005-5007-5.

Harder, J. W., et al. (2005b), The Spectral Irradiance Monitor: Measurement equations and calibration, *Sol. Phys.*, *230*(1–2), 169–204, doi:10.1007/s11207-005-1528-1.

Krivova, N. A., L. Balmaceda, and S. K. Solanki (2007), Reconstruction of solar total irradiance since 1700 from the surface magnetic flux, *Astron. Astrophys.*, *467*, 335–346, doi:10.1051/0004-6361:20066725.

Krivova, N. A., S. K. Solanki, and W. Schmutz (2011), Solar total irradiance in cycle 23, *Astron. Astrophys.*, *529*, A81, doi:10.1051/0004-6361/201016234.

Kushner, P. J., and L. M. Polvani (2004), Stratosphere–troposphere coupling in a relatively simple AGCM: The role of eddies, *J. Clim.*, *17*, 629–639, doi:10.1175/1520-0442(2004)017<0629:SCIARS>2.0.CO;2.

Lean, J. L. (2000), Evolution of the Sun's spectral irradiance since the Maunder minimum, *Geophys. Res. Lett.*, *27*(16), 2425–2428, doi:10.1029/2000GL000043.

Lean, J. L. (2011), How bright is the sun? How does it vary? Why do we care?, *Bull. Am. Meteorol. Soc.*, in press.

Lockwood, M. (2010), Solar change and climate: An update in the light of the current exceptional solar minimum, *Proc. R. Soc. A*, *466*, 303–329, doi:10.1098/rspa.2009.0519.

Lockwood, M., and C. Fröhlich (2007), Recent oppositely directed trends in solar climate forcings and the global mean surface air temperature, *Proc. R. Soc. A*, *463*, 2447–2460, doi:10.1098/rspa.2007.1880.

Lockwood, M., R. Stamper, and M. N. Wild (1999), A doubling of the Sun's coronal magnetic field during the past 100 years, *Nature*, *399*, 437–439, doi:10.1038/20867.

Lockwood, M., M. Owens, and A. P. Rouillard (2009a), Excess open solar magnetic flux from satellite data: 2. A survey of kinematic effects, *J. Geophys. Res.*, *114*, A11104, doi:10.1029/2009JA014450.

Lockwood, M., A. P. Rouillard, and I. D. Finch (2009b), The rise and fall of open solar flux during the current grand solar maximum, *Astrophys. J.*, *700*(2), 937–944, doi:10.1088/0004-637X/700/2/937.

Lockwood, M., R. G. Harrison, T. Woollings, and S. K. Solanki (2010a), Are cold winters in Europe associated with low solar activity?, *Environ. Res. Lett.*, *5*, 024001, doi:10.1088/1748-9326/5/2/024001.

Lockwood, M., C. Bell, T. Woollings, R. G. Harrison, L. J. Gray, and J. D. Haigh (2010b), Top-down solar modulation of climate: Evidence for centennial-scale change, *Environ. Res. Lett.*, *5*, 034008, doi:10.1088/1748-9326/5/3/034008.

Matthes, K., Y. Kuroda, K. Kodera, and U. Langematz (2006), Transfer of the solar signal from the stratosphere to the troposphere: Northern winter, *J. Geophys. Res.*, *111*, D06108, doi:10.1029/2005JD006283.

McClintock, W. E., G. J. Rottman, and T. N. Woods (2000), Solar Stellar Irradiance Comparison Experiment II (SOLSTICE II) for the NASA Earth Observing System's Solar Radiation and Climate Experiment mission, *Proc. SPIE Int. Soc. Opt. Eng.*, *4135*, 225–234, doi:10.1117/12.494220.

McClintock, W. E., G. J. Rottman, and T. N. Woods (2005a), Solar–Stellar Irradiance Comparison Experiment II (SOLSTICE II): Instrument concept and design, *Sol. Phys.*, *230*(1–2), 225–258, doi:10.1007/s11207-005-7432-x.

McClintock, W. E., M. Snow, and T. N. Woods (2005b), Solar–Stellar Irradiance Comparison Experiment II (SOLSTICE II): Pre-launch and on-orbit calibrations, *Sol. Phys.*, *230*(1–2), 259–294, doi:10.1007/s11207-005-1585-5.

Perlwitz, J., and N. Harnik (2003), Observational evidence of a stratospheric influence on the troposphere by planetary wave reflection, *J. Clim.*, *16*, 3011–3026, doi:10.1175/1520-0442(2003)016<3011:OEOASI>2.0.CO;2.

Plumb, R. A., and K. Semeniuk (2003), Downward migration of extratropical zonal wind anomalies, *J. Geophys. Res.*, *108*(D7), 4223, doi:10.1029/2002JD002773.

Rottman, G. (2000), Variations of solar ultraviolet irradiance observed by the UARS SOLSTICE—1991 to 1999, *Space Sci. Rev.*, *94*(1/2), 83–91, doi:10.1023/A:1026786315718.

Rozanov, E., T. Egorova, C. Fröhlich, M. Haberreiter, T. Peter, and W. Schmutz (2002), Estimation of the ozone and temperature sensitivity to the variation of spectral solar flux, in *Proceedings of the SOHO 11 Symposium on From Solar Min to Max: Half a Solar Cycle with SOHO*, edited by A. Wilson, *Eur. Space Agency Spec. Publ.*, *ESA-SP 508*, 181–184.

Russell, C. T., J. G. Luhmann, and L. K. Jian (2010), How unprecedented a solar minimum?, *Rev. Geophys.*, *48*, RG2004, doi:10.1029/2009RG000316.

Scaife, A. A., J. R. Knight, G. K. Vallis, and C. K. Folland (2005), A stratospheric influence on the winter NAO and North Atlantic surface climate, *Geophys. Res. Lett.*, *32*, L18715, doi:10.1029/2005GL023226.

Shindell, D. T., G. A. Schmidt, R. L. Miller, and D. Rind (2001), Northern Hemisphere winter climate response to greenhouse gas, ozone, solar, and volcanic forcing, *J. Geophys. Res.*, *106*(D7), 7193–7210, doi:10.1029/2000JD900547.

Simpson, I. R., M. Blackburn, and J. D. Haigh (2009), The role of eddies in driving the tropospheric response to stratospheric heating perturbations, *J. Atmos. Sci.*, *66*, 1347–1365, doi:10.1175/2008JAS2758.1.

Snow, M., W. E. McClintock, and T. N. Woods (2010), Solar spectral irradiance variability in the ultraviolet from SORCE and UARS SOLSTICE, *Adv. Space Res.*, *46*(3), 296–302, doi:10.1016/j.asr.2010.03.027.

Wang, Y.-M., J. L. Lean, and N. R. Sheeley Jr. (2005), Modeling the Sun's magnetic field and irradiance since 1713, *Astrophys. J.*, *625*(1), 522–538, doi:10.1086/429689.

Wenzler, T., S. K. Solanki, and N. A. Krivova (2009), Reconstructed and measured total solar irradiance: Is there a secular trend between 1978 and 2003?, *Geophys. Res. Lett.*, *36*, L11102, doi:10.1029/2009GL037519.

Willson, R. C., and A. V. Mordvinov (2003), Secular total solar irradiance trend during solar cycles 21–23, *Geophys. Res. Lett.*, *30*(5), 1199, doi:10.1029/2002GL016038.

Woods, T. N., et al. (1996), Validation of the UARS solar ultraviolet irradiances: Comparison with the ATLAS 1 and 2 measurements, *J. Geophys. Res.*, *101*(D6), 9541–9569, doi:10.1029/96JD00225.

Woods, T., G. Rottman, C. Russell, and B. Knapp (1998), In-flight degradation results for the UARS SOLSTICE instrument, *Metrologia*, *35*(4), 619–623, doi:10.1088/0026-1394/35/4/68.

Woods, T. N., et al. (2000), TIMED Solar EUV experiment, *Phys. Chem. Earth, Part C*, *25*(5–6), 393–396, doi:10.1016/S1464-1917(00)00040-4.

Woollings, T., M. Lockwood, G. Masato, C. Bell, and L. Gray (2010), Enhanced signature of solar variability in Eurasian winter climate, *Geophys. Res. Lett.*, *37*, L20805, doi:10.1029/2010GL044601.

M. Lockwood, Space Environment Physics Group, Department of Meteorology, University of Reading, Earley Gate, P.O. Box 243, Reading, Berkshire, RG6 6BB, UK. (m.lockwood@reading.ac.uk)